Cell PRESS
Developmental Cell
Article

Notch Initiates the Endothelial-to-Mesenchymal Transition in the Atrioventricular Canal through Autocrine Activation of Soluble Guanylyl Cyclase

Alex C.Y. Chang,[1] YangXin Fu,[1,7] Victoria C. Garside,[2] Kyle Niessen,[1] Linda Chang,[1] Megan Fuller,[1,5] Audi Setiadi,[1] Justin Smrz,[1] Alastair Kyle,[3] Andrew Minchinton,[3,5] Marco Marra,[1,6] Pamela A. Hoodless,[2,6] and Aly Karsan[1,4,5,*]
[1]Michael Smith Genome Sciences Centre
[2]Terry Fox Laboratory
[3]Department of Integrative Oncology-Radiation Biology Unit
[4]Cancer Genetics Laboratory
British Columbia Cancer Agency, Vancouver BC V5Z 1L3, Canada
[5]Department of Pathology and Laboratory Medicine
[6]Department of Medical Genetics
University of British Columbia, Vancouver BC V6T 2B5, Canada
[7]Present address: Department of Obstetrics and Gynecology, Department of Oncology, and Faculty of Medicine and Dentistry, University of Alberta, Edmonton AB T6G 1Z2, Canada
*Correspondence: akarsan@bccrc.ca
DOI 10.1016/j.devcel.2011.06.022

SUMMARY

The heart is the most common site of congenital defects, and valvuloseptal defects are the most common of the cardiac anomalies seen in the newborn. The process of endothelial-to-mesenchymal transition (EndMT) in the cardiac cushions is a required step during early valve development, and Notch signaling is required for this process. Here we show that Notch activation induces the transcription of both subunits of the soluble guanylyl cyclase (sGC) heterodimer, GUCY1A3 and GUCY1B3, which form the nitric oxide receptor. In parallel, Notch also promotes nitric oxide (NO) production by inducing Activin A, thereby activating a PI3-kinase/Akt pathway to phosphorylate eNOS. We thus show that the activation of sGC by NO through a Notch-dependent autocrine loop is necessary to drive early EndMT in the developing atrioventricular canal (AVC).

INTRODUCTION

During cardiac development, the linear heart tube loops rightward at embryonic day (E) 8.5 to initiate the establishment of a four-chambered structure (E9.0–9.5) consisting of paired left and right atria, and ventricles. In order to separate the chambers, swellings composed of extracellular matrix in the atrioventricular canal (AVC) and the outflow tract, referred to as cardiac cushions, become populated by mesenchymal cells generated from the overlying endocardium. This process called endothelial-to-mesenchymal transition (EndMT) commences at E9.5 in the AVC, resulting in endocardial cells (ECs) delaminating from the monolayer and invading the underlying matrix (Camenisch et al., 2002). Following remodeling, the cushions eventually develop into the cardiac valves and the membranous septum of the adult heart (Eisenberg and Markwald, 1995; Niessen and Karsan, 2008).

Several signaling pathways coordinate to initiate and potentiate EndMT, with the Notch pathway being a central player in the process (Niessen and Karsan, 2008; Timmerman et al., 2004). Notch proteins are a family of transmembrane receptors (*Notch1–4* in mammals) that are activated upon binding by Notch ligands: Jagged (Jag) 1 and 2 and Delta-like (Dll) 1, 3, and 4. Upon activation, Notch receptors undergo proteolytic processing, and the intracellular domain of Notch (NICD) is released from its membrane tether. The NICD then translocates to the nucleus, binds to the DNA-binding corepressor *RBPJ* (recombination signal-binding protein for immunoglobulin κ J region), and recruits the coactivator *MAML1* (Mastermind-like 1), to derepress and activate transcription of downstream target genes such as the *HES* and *HEY* family of transcription factors (Iso et al., 2003). Deletion of *Notch1* or *Rbpj* in mice results in malformation of the cardiac cushions (Timmerman et al., 2004). Deletion of the Notch target gene *Hey2*, or double deletion of *Hey1* and *Hey2* or *Hey1* and *HeyL*, results in various congenital heart defects, including cardiac cushion defects (Donovan et al., 2002; Fischer et al., 2004, 2007). Mutations of *Notch1* are associated with nonsyndromic valvular disease such as bicuspid aortic valves, as well as with more severe cardiac anomalies (Garg et al., 2005). Mutations in *Jag1* have been implicated in Alagille syndrome, an entity that comprises a spectrum of defects including pulmonary artery stenosis, tetralogy of Fallot, and additional valvular anomalies (Eldadah et al., 2001; Li et al., 1997; Oda et al., 1997).

Nitric oxide (NO) has also been shown to play a role in cardiac function (Fukumura et al., 2006; Rastaldo et al., 2007), blood pressure homeostasis (Sessa, 2009), and epithelial-mesenchymal transition (Vyas-Read et al., 2007). NO is generated by nitric oxide synthases (NOSs), of which there are three isoforms: endothelial (*eNOS*, or *NOS3*), inducible (*iNOS*, or *NOS2*) and neuronal (*nNOS*, or *NOS1*). External signals (shear

stress, calcium influx, or growth factors) culminate in phosphorylation events that can either activate (Ser114 and Ser1177) or inhibit (Thr485) *eNOS* (Mount et al., 2007). Similar to heterozygous NOTCH1 mutations in human (Garg et al., 2005), homozygous *eNOS* knockout mice also display bicuspid aortic valves and other major cardiac anomalies (Aicher et al., 2007; Feng et al., 2002; Lee et al., 2000). Of the three classes of type III guanylyl cyclases (GCs), NO signaling is propagated through the soluble GC (sGC) heterodimer (Baker and Kelly, 2004; Yamagami and Suzuki, 2005), which consists of an α subunit (*GUCY1A2* or *GUCY1A3*) and a β subunit (*GUCY1B3*). *GUCY1A3/1B3* is expressed in most tissues, whereas *GUCY1A2/1B3* is predominantly found in the brain (Giuili et al., 1992; Mergia et al., 2003). Activation of sGC leads to production of the second messenger 3′, 5′ cyclic guanosine monophosphate (cGMP), which results in smooth muscle cell relaxation by blocking calcium influx and dephosphorylation of myosin light chains (Ignarro et al., 1986; Murad, 1986). In addition to blood pressure regulation, sGC proteins have also been shown to promote endothelial cell survival and migration (Pyriochou et al., 2006; Pyriochou et al., 2007a, 2007b).

In this study we demonstrate that Notch induces activation of the NO-sGC axis through an autocrine loop during EndMT in the AVC. The promoters of both *GUCY1A3* and *GUCY1B3* are bound by RBPJ, and transcription is induced upon Notch activation. Inhibition of Notch specifically in endocardial cells in vivo inhibits EndMT and decreases *Gucy1b3* expression. Similarly, sGC inhibition blocks EndMT in AVC explants and decreases cushion cellularization at E9.5 and E10.5 in vivo. Concomitant with upregulation of the *GUCY* genes, Notch induces Activin A, which in turn activates PI3K and Akt in a paracrine fashion followed by downstream eNOS activation and NO production. Here we show that Notch signaling increases NO production simultaneously with induction of the NO receptor sGC, and this pathway contributes to EndMT in the AVC.

RESULTS

GUCY1A3 and *GUCY1B3* Are Notch Target Genes

To identify Notch target genes in the AVC endocardium during heart development, we compared two microarray data sets with AVC transcriptome libraries. Transcripts induced by at least 2-fold in NICD-transduced human umbilical vein endothelial cells (HUVECs; this study), and in *Dll4*-activated HUVEC (Harrington et al., 2008), were compared with mRNA expressed in the AVC at E9.5, E10.5, and E11.5 as determined by Serial Analysis of Gene Expression (SAGE) (Siddiqui et al., 2005; Vrljicak et al., 2010). Of the 24 candidate genes identified (see Figure S1A available online), 11 transcripts were upregulated in human ECs transduced with Notch ligands (Jag1 or Dll4) or NICD compared to the empty vector control using reverse transcription-quantitative polymerase chain reaction (RT-qPCR) (Table S1).

Of the 11 validated candidates, 5 have been reported to be associated with heart development, EndMT, or are regulated by Notch signaling (*Hey1*, *Jag1*, SDC*1*, SDC*2*, and *SNAI2*) (Arrington and Yost, 2009; Fischer et al., 2004, 2007; High et al., 2008b; Niessen et al., 2008; Sun et al., 1998). Of the remaining six candidates, *GUCY1A3* and *GUCY1B3* were selected for further study because both genes are highly induced by Notch signaling (Table S1) and heterodimerize to form the soluble NO receptor, sGC. RT-qPCR showed that Notch activation by ligand-induced activation (Jag1, Dll4) or enforced expression of NICD increased *GUCY1A3* mRNA levels 316 ± 43, 18 ± 1.5, and 313 ± 43.8-fold, respectively, and *GUCY1B3* mRNA levels by 154 ± 3.2, 13.4 ± 1.7, and 282 ± 37.2-fold, respectively (Figure 1A). As a positive control, we confirmed that the known Notch target gene *HEY1* was also induced by Notch activation (Figure 1A). Induction of *GUCY1A3* and *GUCY1B3* mRNA was abolished when Jag1- or Dll4-expressing ECs were treated with the γ-secretase inhibitor, N-[N-(3,5-difluorophenacetyl)-l-alanyl]-S-phenylglycine t-butyl ester (DAPT) (Figure 1B), thus confirming Notch-dependent induction.

To determine whether the ligand-expressing or Notch-activated cells induce sGC, ligand-expressing Jag1 or Dll4 (YFP^+) was cocultured with parental ECs (YFP^-) and flow sorted after 48 hr into YFP^+ (ligand-expressing cells) and YFP^- (parental cells) populations, and each population was analyzed by RT-qPCR. As noted by induction of *ACTA2* and *HEY1* (Figure 1C), Notch activation occurs mainly in the parental cells in this coculture system. The major induction of *GUCY1A3* and *GUCY1B3* mRNA levels also occurred in the YFP^- parental cells (Figure 1D), consistent with the notion that *GUCY1A3* and *GUCY1B3* are induced by Notch activation. Although TGFβ signaling plays a crucial role in AVC development (Camenisch et al., 2002), TGFβ1 stimulation had little effect on *GUCY1A3* and *GUCY1B3* expression, and did not synergize with Notch activation to induce sGC components (Figure S1B).

Analysis of the human and mouse *GUCY1A3* and *GUCY1B3* promoters (from 1.5 kb upstream of the transcriptional start site [TSS] to the end of intron 1) revealed several putative *RBPJ*-binding sites (Figure S1C). Five putative *RBPJ*-binding sites were identified in the human *GUCY1B3* promoter, and three of these sites were conserved in the mouse, while only one conserved putative *RBPJ*-binding site was noted between the human and murine *GUCY1A3* promoters. Chromatin immunoprecipitation (ChIP) followed by qPCR with primers flanking the *RBPJ* elements demonstrated that RBPJ bound all three conserved RBPJ consensus motifs in the human GUCY1B3 promoter (−1065, 6.7 ± 2.1-fold; −37, 2.6 ± 0.4-fold; +247, 3.4 ± 0.9-fold) as well as the single conserved *RBPJ* consensus motif in the human GUCY1A3 promoter (−944, 4.4 ± 1.7-fold) (Figure 1E) in ECs transduced with Flag-tagged RBPJ. As a positive control, we showed RBPJ binding to the human *HEY1* promoter located 180 bp upstream of the TSS (Figure 1E). As a negative control, we used the *ZNF3* promoter, which lacks a consensus RBPJ-binding motif (Figure 1E). Immunoblotting of ECs activated by NICD, Jag1, or Dll4 showed that Notch activation induced GUCY1B3 protein (Figure 1F), and the induction was abolished when RBPJ was knocked down (Figure 1G). Thus, *GUCY1A3* and *GUCY1B3* are Notch target genes activated by an RBPJ-dependent mechanism.

To demonstrate that *Gucy1b3* is a target gene of Notch in vivo, an EC-specific Tet-inducible binary transgenic mouse model was used where expression of a pan-Notch inhibitor, dominant-negative (dn)-MAML fused to GFP behind the Tet^{OS} promoter, is driven by the VE-cadherin promoter (VEtTA) in the

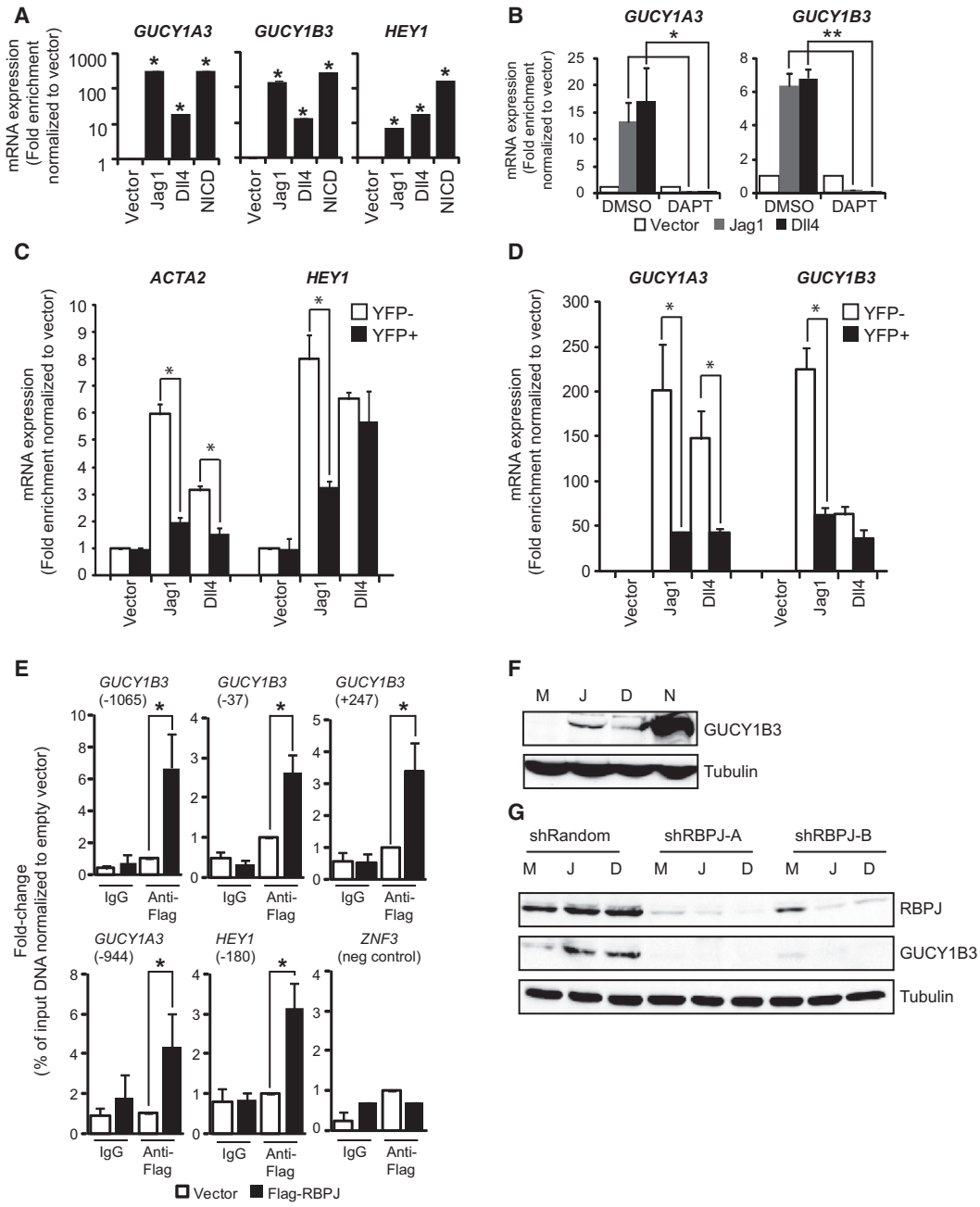

Figure 1. Notch Signaling Induces *GUCY1A3* and *GUCY1B3* Expression through RBPJ

(A and B) Expression of *GUCY1A3* and *GUCY1B3* (see Figure S1) was induced (A) as determined by RT-qPCR in ECs transduced with Jag1, Dll4, NICD, or empty vector, but blocked (B) by the γ-secretase inhibitor, DAPT (10 μM), compared to vehicle (DMSO). Data are shown as fold enrichment over the empty vector control (n = 3; *p = 0.05, **p = 0.001).

(C and D) Parental ECs (YFP^-) cocultured with Notch ligands (YFP^+) for 48 hr were flow sorted for YFP expression and analyzed by RT-qPCR for expression of *ACTA2* and *HEY1* (C), or *GUCY1A3* and *GUCY1B3* (D) in the YFP^+ (ligand-expressing) and YFP^- (parental ECs) cells. Data are shown as fold enrichment over the empty vector control (n = 3; *p = 0.05).

(E) RBPJ occupancy of conserved RBPJ-binding sites of human *GUCY1B3* and *GUCY1A3* promoters (Figure S2B) was examined by anti-Flag ChIP with IgG ChIP used as a negative control in ECs transduced with either Flag-RBPJ or empty vector. qPCR of the immunoprecipitated DNA was conducted using primers flanking the conserved RBPJ-binding sites. Fold enrichment was calculated by normalizing to input DNA and then referencing to empty vector anti-Flag ChIP (n = 5; *p = 0.05).

(F) Cell lysates from ECs transduced with Jag1 (J), Dll4 (D), NICD (N), or empty vector (M) were immunoblotted for GUCY1B3 protein.

(G) Notch-activated cells were lentivirally transduced with shRBPJ-A, shRBPJ-B, or shRandom (control) and immunoblotted for GUCY1B3 and RBPJ protein. Tubulin expression was used as a loading control.

absence of tetracycline (Fu et al., 2009). To assay Gucy1b3 protein expression during EndMT, EC Notch inhibition was induced at E9.5 by withdrawal of tetracycline from the drinking water, and embryos were collected at E10.5 (VEtTA × Tet^{OS}-dnMAML-GFP). In VEtTA×Tet^{OS}-dnMAML-GFP E10.5 double-transgenic hearts, Gucy1b3 protein expression was reduced in both the endocardium and the mesenchyme of the AVC compared to single transgenic littermate controls (Figures 2A–2H). Notch inhibition resulted in an approximately 2-fold reduction in the intensity of Gucy1b3 staining in the AVC when normalized to DAPI staining intensity (1.9 ± 0.2 versus 0.8 ± 0.2; p = 0.02) or to cellularity (number of nuclei, 2.5 ± 0.2 versus 1.4 ± 0.2; p = 0.003). Reduced Gucy1b3 staining was also noted specifically in the endocardium as determined relative to CD31 staining intensity (1.3 ± 0.1 versus 0.6 ± 0.1; p = 0.005) (Figure 2I). These results suggest that *Gucy1b3* expression is regulated by Notch in the developing AVC and that inhibition of EC-Notch signaling blocks *Gucy1b3* expression in vivo.

Notch-Induced sGC Drives EndMT

To determine the role of sGC in EndMT, we used an ex vivo AVC explant model in which E9.5 wild-type AVCs are cultured on collagen gels, and cellular migration and invasion of the matrix are quantified 48 hr later (Camenisch et al., 2002; Niessen et al., 2008). To ensure that the migrating/invading cells comprised mesenchymal cells, all explants were also stained with the mesenchymal marker, SMA, and the areas of SMA and DAPI staining were correlated (Figure S2). Inhibition of sGC activity with [1H-[1,2,4]oxadiazolo-[4, 3-a]quinoxalin-1-one] (ODQ; 10 μM) resulted in significant blockade of EndMT ($p < 0.05$), similar to Notch inhibition (DAPT 10 μM; $p < 0.05$), compared to vehicle-treated explants (Figure 2J). In contrast, administration of the NO-independent sGC activator BAY41-2272 (10 μM) showed marked induction of EndMT ($p < 0.05$; Figure 2J). Additionally, knockdown of *Gucy1b3* in AVC explants using lentiviral transduction with two distinct shRNAs targeting different sequences of *Gucy1b3* significantly reduced EndMT compared to a vector control ($p < 0.05$) (Figure 2K). To determine whether sGC activity is required for cushion cellularization in vivo, ODQ (50 mg/kg) was administered to pregnant C57Bl/6J mice intraperitoneally 24 hr prior to embryo isolation. Cushion cellularization was significantly inhibited at E9.5 when ODQ was administered at E8.5 (vehicle, 43.1 ± 6.6 nuclei/μm^2; ODQ, 21.3 ± 6.2 nuclei/μm^2; p = 0.02) and at E10.5 with ODQ administered at E9.5 (vehicle, 170.5 ± 4.4 nuclei/μm^2; ODQ, 149.4 ± 3.7 nuclei/μm^2; p = 0.002), but not at E11.5 when EndMT is complete (vehicle, 270.1 ± 17.5 nuclei/μm^2; ODQ, 289.5 ± 14.9 nuclei/μm^2) (Figures 2L and 2M). Taken together, these results demonstrate that sGC activation is required for EndMT during the initiation of cushion cellularization.

Notch Activates NO Synthesis in a Cell Nonautonomous Fashion

Given that sGC is activated by NO, we examined whether Notch also induces NO synthesis in order to activate the sGC pathway in an autocrine fashion. Enforced expression of NICD or coculture of parental ECs with Notch ligand-expressing cells increased NO production compared to vector-transduced cells, as measured by accumulation of the NO-reactive dye diaminorhodamine 4M-AM (DAR4M-AM) (Figure 3A). The majority of NO accumulation was observed in Notch-activated cells. However, NO accumulation was also noted in the non-Notch-activated ECs, suggesting a potential paracrine effect of Notch activation. NO induction was abolished when ECs were treated with the pan-NOS inhibitor Nω-Nitro-L-arginine methyl ester hydrochloride (L-NAME), thereby confirming the requirement of NOS activity (Figure 3A). Coculture of parental ECs with Notch Jag1-expressing cells also increased NO production, as quantified by the Griess reaction (p = 0.002; Figure 3B). To assay for the degree of sGC activation, we measured cGMP concentration in the cell lysates. Cell lysates from coculture of parental ECs with Jag1- or Dll4-transduced ECs showed a significant increase in cGMP (0.21 ± 0.06 and 0.26 ± 0.08 cGMP [pmol/ml]/total protein [μg], respectively) compared to cocultures with the empty vector control (0.07 ± 0.02 cGMP [pmol/ml]/total protein [μg]; p = 0.05) (Figure 3C).

To confirm a paracrine effect of Notch on NO synthesis, ECs were treated with conditioned medium collected from NICD- or vector-transduced ECs. Intracellular NO staining with DAR4M-AM showed accumulation of NO in NICD-conditioned medium-exposed ECs over time (Figure 3D), with a significant increase in NO generation, as measured by the Griess reaction, compared to vector-conditioned medium-treated controls following 90 and 120 min of exposure (1.7 ± 0.1 versus 1.4 ± 0.1 μM nitrite/μg protein [p = 0.05] and 1.8 ± 0.1 versus 1.3 ± 0.1 μM nitrite/μg protein [p = 0.05], respectively) (Figure 3E). Cell lysates treated with NICD-conditioned medium also showed a significant increase in sGC activation as determined by an increase in cGMP compared to vector-conditioned medium-exposed ECs following 90 and 120 min of exposure (3.2 ± 1.0 versus 1.1 ± 0.6 cGMP [pmol/ml]/total protein [μg] [p = 0.05], and 3.3 ± 0.7 versus 1.2 ± 0.5 cGMP [pmol/ml]/total protein [μg] [p = 0.05], respectively) (Figure 3F). Thus, Notch activation induces NO synthesis in a paracrine fashion to activate sGC.

To observe NO production in the developing AVC, DAR4M-AM (25 μmol/kg) was administered intraperitoneally into pregnant mice 1 hr prior to embryo isolation. In the AVC, DAR4M-AM fluorescence was observed in the endocardium and mesenchyme at E10.25 and E10.5 (Figure 3G). In contrast, NO was weakly detectable with DAR4M-AM at E10.25 and E10.5 when Notch signaling was inhibited, by removal of tetracycline from the drinking water 24 hr prior in VEtTAxTet^{OS}-dnMAML-GFP double transgenic embryos compared to littermate controls (Figure 3G). Quantification of DAR4M-AM staining relative to the AVC cushion area showed a 2.7- and 5.6-fold decrease of NO in E10.25 and E10.5 VEtTAxTet^{OS}-dnMAML-GFP AVC compared to littermate controls (E10.25, 176 ± 24 versus 474 ± 70.9; E10.5, 298 ± 103 versus 53.6 ± 10.7 positive-pixels normalized to AVC area analyzed [p = 0.002]) (Figure 3H). Quantification of DAR4M-AM staining in the endocardium showed a 1.3- and 12.8-fold decrease of NO in E10.25 and E10.5 VEtTAxTet^{OS}-dnMAML-GFP AVC compared to littermate controls (E10.25, 0.41 ± 0.006 versus 0.30 ± 0.04; E10.5, 0.66 ± 0.35 versus 0.056 ± 0.02 positive-pixels normalized to endocardial area [p = 0.05]) (Figure 3I). Taken together, these results demonstrate that Notch induces NO production in the developing AVC in a paracrine manner, which is then capable of stimulating the sGC heterodimer formed by Gucy1a3 and Gucy1b3, in Notch-activated ECs.

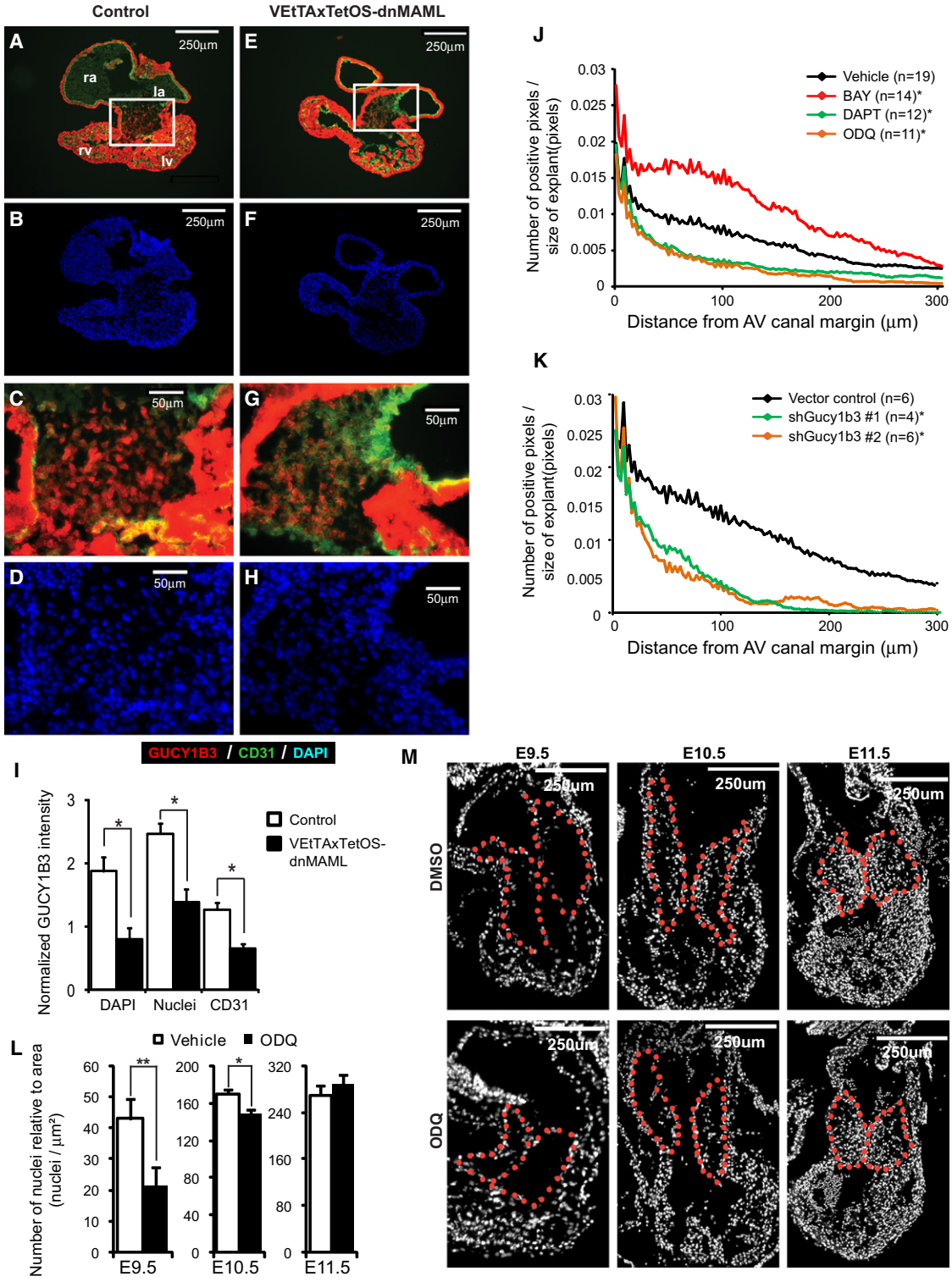

Figure 2. Notch-Induced sGC Contributes to the Initiation of EndMT

(A–H) GUCY1B3 (red) and CD31 (green) protein expression was evaluated by immunofluorescent staining (A, C, E, and G) relative to DAPI staining (B, D, F, and H) in E10.5 littermate controls (A–D) and VEtTAxTet^{OS}-dnMAML AVC (E–H). Boxes in (A) and (E) are regions that have been enlarged and presented as (C) and (D) and (G) and (H).

(I) Intensity of immunofluorescence staining of GUCY1B3 relative to DAPI intensity, number of nuclei, or CD31 intensity (only EC staining quantified) is shown (*p = 0.005) (n = 14 littermate control and 4 VEtTAxTet^{OS}-dnMAML-GFP embryos; three sections per embryo were used for quantification).

Notch-Induced Activin A Activates eNOS and Promotes EndMT

To identify the paracrine factor responsible for NO induction in the developing AVC that is regulated by Notch, we used gene ontology classifications to select ten secreted factors as candidate genes that were present both in the EC NICD microarray and the AVC transcriptome data sets (Figure 4A). Using RT-qPCR of NICD-transduced ECs, parental ECs cocultured with Notch ligand-expressing (Jag1, Dll4) ECs, and vector-transduced ECs, we validated Inhibin β A (*INHBA*), the gene that encodes the subunits of the homodimer Activin A, and Insulin Growth Factor 2 (*IGF2*), as two factors that were induced by both NICD and ligand activation of Notch. To confirm that the products of these genes were secreted, we measured protein concentrations of Activin A and IGF2 by ELISA in serum-free NICD-conditioned medium. We did not detect IGF2 protein (data not shown), but Activin A was significantly increased in NICD-conditioned medium compared to the empty vector conditioned medium (9.11 ± 0.28 versus 0.05 ± 0.01 ng/ml [$p = 0.001$], respectively) (Figure 4B). By RT-qPCR we confirmed that ligand-mediated induction of *INHBA* was Notch dependent because either Jag1- or Dll4-induced *INHBA* expression was inhibited by a γ-secretase inhibitor (DAPT) ($p = 0.005$; Figures 4C and 4D). In contrast, TGFβ1 had no effect on *INHBA* expression (Figure S3A). One conserved putative RBPJ-binding site located in intron 1 of human *INHBA* was identified (+1018 bp from TSS), and anti-Flag ChIP-qPCR confirmed RBPJ binding to the human *INHBA* promoter in ECs transduced with Flag-RBPJ relative to the empty vector (2.0 ± 0.1-fold enrichment; $p = 0.05$) (Figure 4E). To assay *Inhba* expression in vivo, E9.5, E10.5, and E11.5 AVCs and whole hearts were harvested for RT-qPCR. mRNA of *Inhba* and its receptors (*Acvr2a*, *Acvr2b*, *Acvr1b*, and *Acvr1c*) was detected in the AVC from E9.5 to E11.5, with a significant increase in *Inhba* expression at E9.5 and E10.5 in the AVC compared to the whole heart ($p = 0.05$; Figures 4F–4H). To confirm that *Inhba* is a target gene of Notch in vivo, we performed in situ hybridization on E10.5 VEtTAxTet^{OS}-dnMAML-GFP and littermate controls, which showed a marked decrease in *Inhba* expression following Notch blockade (Figure S3B). Collectively, these data indicate that Notch activation drives expression of *INHBA* and production of the INHBA homodimer, Activin A.

To determine whether Activin A is capable of activating eNOS, parental ECs were treated with recombinant Activin A. eNOS activation (as determined by anti-phospho-eNOS-Ser1177 immunoblotting) was detected as early as 15 min following Activin A stimulation (Figure 5A). Activin A stimulated eNOS activation through PI3K/Akt, because inhibitors targeting either PI3K (LY294002, 10 μM) or Akt (Triciribine, 10 μM) blocked eNOS phosphorylation (Figure 5B). Activin A significantly induced NO accumulation, as determined by the Griess reaction, and this induction of NO was abolished when ECs were transduced with a dnAkt ($p = 0.05$; Figure 5C).

To determine whether an eNOS-activating factor is secreted from Notch-activated cells, we treated ECs with NICD-conditioned medium and immunoblotted cell lysates for phospho-eNOS-Ser1177. We detected eNOS activation as early as 15 min following stimulation compared to the empty vector control (Figure 5D). eNOS activation was associated with Akt activation (p-Akt) (Figure 5D). Pretreatment with LY294002 (10 μM), Triciribine (10 μM), or a neutralizing anti-Activin A antibody (5 ng/ml) blocked the ability of NICD-conditioned medium to activate eNOS (Figure 5E). Furthermore, treating dnAkt-transduced ECs with NICD-conditioned medium failed to activate eNOS (Figure 5F), suggesting an Akt-dependent activation. We thus conclude that NICD-conditioned medium activates eNOS via a PI3K/Akt mechanism through the induction and secretion of Activin A.

To confirm the direct role of Activin A-induced NO in cardiac cushion EndMT, AVC explants treated with L-NAME (50 μM; $p < 0.05$), LY294002 (10 μM; $p < 0.05$), or Triciribine (10 μM; $p < 0.05$) showed significant inhibition of EndMT compared to vehicle treatment (Figures 6A and S4). Moreover, AVC isolated from eNOS$^{-/-}$ mice exhibited pronounced decrease in EndMT compared to wild-type AVC ($p < 0.05$; Figure 6B). Similarly, neutralizing anti-Activin A antibody (5 ng/ml) also inhibited EndMT in AVC explants compared to the IgG control ($p < 0.05$; Figures 6C and S5). Significant EndMT inhibition was also observed in AVC treated with short-hairpin lentivirus targeting *Inhba* compared to vector control ($p < 0.05$; Figures 6D and S5). These data support a model where Notch-induced Activin A stimulates NO synthesis via eNOS activation to promote EndMT.

DISCUSSION

In the developing embryo, the heart is the first organ to form. EndMT commences in the AVC at E9.5 with the cellularized cushions eventually giving rise to the membranous interventricular septum and the heart valves (High and Epstein, 2008a; Niessen and Karsan, 2008). Dysregulation of the Notch signaling pathway is associated with various cardiovascular anomalies and has been found to be essential for EndMT during AVC development (Timmerman et al., 2004; reviewed in High and Epstein, 2008a; Niessen and Karsan, 2008). However, very few Notch target genes that facilitate cardiovascular development have been reported. Notch signaling can induce EndMT by induction of transcription factors *Snail* (Luna-Zurita et al., 2010; Timmerman et al., 2004) and *Slug* (Niessen et al., 2008; Noseda et al., 2004) and regulating of TGFβ signaling via *Smad3* in the developing AVC (Fu et al., 2009). In this study, we show that

(J) Quantitative analysis of EndMT in AVC explants from E9.5 wild-type mice treated with BAY41-2272 (10 μM), DAPT (10 μM), ODQ (10 μM), or vehicle as determined by automated image analysis 48 hr postexplant.

(K) AVC explants from E9.5 wild-type mice were lentivirally transduced with two distinct shGucy1b3 constructs (#1 & #2) or vector control. Results represent the distance migrated by cells emanating from the edge of the AVC explant normalized to the area of the AVC explant (*$p < 0.001$). See also Figure S3 for correlation with Acta2 immunostaining for (J) and (K).

(L and M) ODQ (50 mg/kg) was administered intraperitoneally 24 hr prior to collection of E9.5–E11.5 embryos (L). Cellularity of the AVC was determined by quantifying the number of nuclei relative to the area of the AVC ($n = 10$, for each time point; *$p = 0.05$, **$p = 0.002$), and representative micrographs are shown in (M).

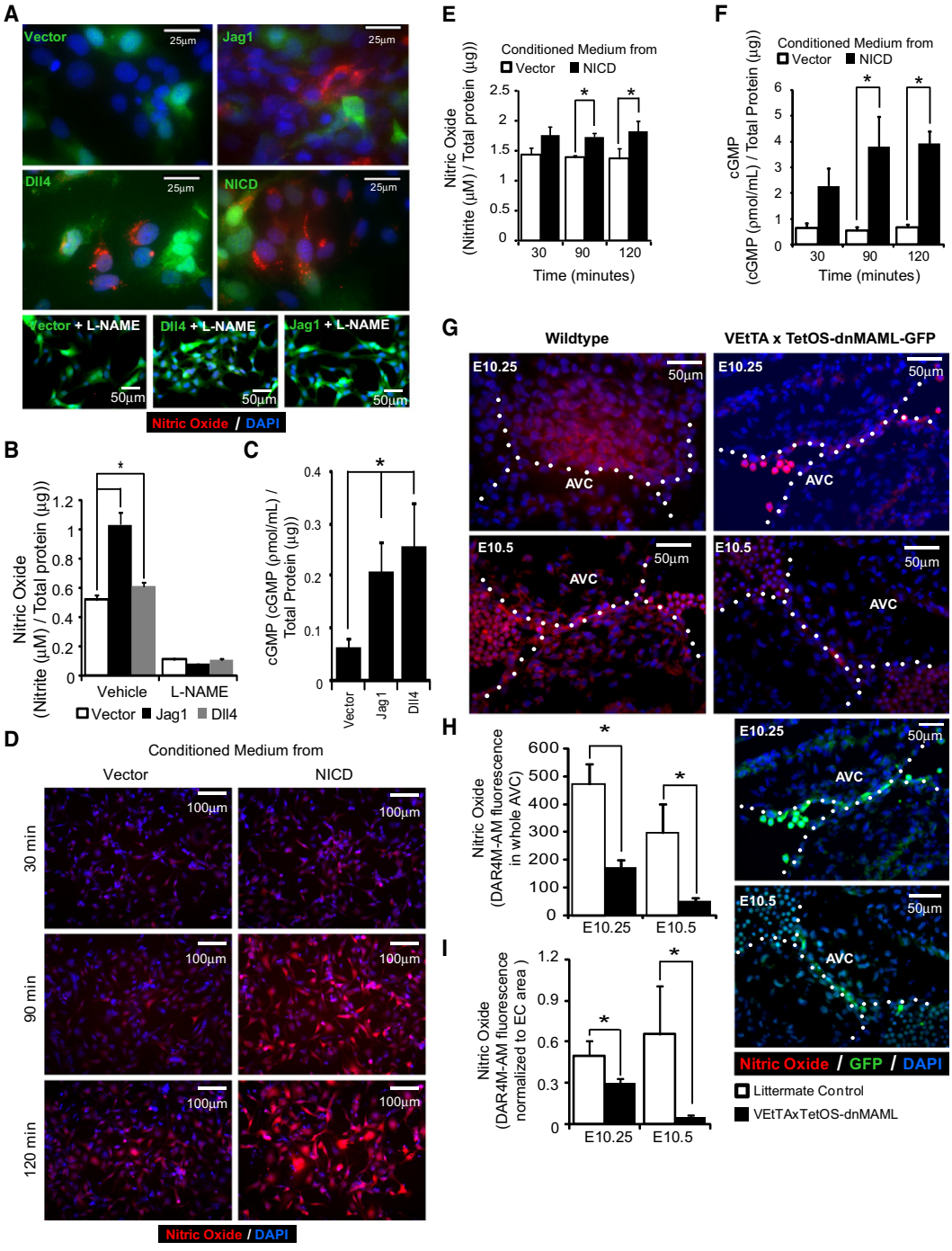

Figure 3. Notch Activation Results in NO Production in a Cell Nonautonomous Fashion

(A) Coculture of Notch ligand-expressing (Jag1-YFP or Dll4-YFP), NICD-YFP-expressing, or vector-YFP ECs with parental ECs induces NO as visualized by DAR4M-AM fluorescence (red). YFP fluorescence (green) highlights the transduced cells, which represent either ligand-expressing, NICD-expressing, or vector-transduced ECs, cocultured with the non-YFP parental ECs. The pan-NOS inhibitor L-NAME (50 μM) was used as a control to confirm NOS dependence of NO production (lower panels).

(B) Mean nitrite levels as measured by the Griess reaction normalized to the total amount of protein in Jag1, Dll4, or vector-transduced ECs cocultured with parental ECs treated with either L-NAME (50 μM) or vehicle (n = 5; *p = 0.002).

(C) Mean cGMP levels normalized to the total amount of protein in Jag1, Dll4, or vector-transduced ECs cocultured with parental ECs (n = 7; *p = 0.05).

(D–F) Induction of NO and downstream activation of sGC in ECs treated with NICD-conditioned medium. NO level and activity at different times following NICD-conditioned medium exposure were assayed by DAR4M-AM staining (D), Griess reaction (E; n = 4; *p = 0.05), and cGMP ELISA (F; n = 4; *p = 0.05).

Notch promotes EndMT by autocrine activation of NO signaling. Notch activation induces expression of the two components of the heterodimeric sGC, *Gucy1a3* and *Gucy1b3*, in the transitioning endocardium. In addition, Notch-activated ECs secrete Activin A, leading to activation of eNOS and release of NO by a PI3K/Akt-dependent mechanism. Recent findings support a role for Akt in promoting EndMT in the AVC (Feng et al., 2010; Meadows et al., 2009).

Although *Gucy1a3* or *Gucy1a2* single gene-targeted mice exhibit only a mild phenotype (Mergia et al., 2006), *Gucy1b3*-targeted mice are hypertensive and demonstrate platelet defects, and impaired peristalsis (Friebe et al., 2007; Groneberg et al., 2010). Thus, it is thought that Gucy1a2 and Gucy1a3 can compensate for each other in the context of embryonic gene targeting, but Gucy1b3 is the essential partner for both Gucy1a isoforms. Although NO signaling in the vasculature is best recognized for relaxing vascular smooth muscle through activation of sGC, *Gucy1a3* and *Gucy1b3* proteins have also been shown to play a role in cell migration during angiogenesis in zebrafish (Pyriochou et al., 2006). Our findings reported here are in keeping with a role for sGC in promoting endothelial migration and invasion in the context of EndMT during AVC development, as seen in angiogenesis. Indeed, the process of angiogenesis requires that ECs delaminate and invade the underlying matrix similar to the process of EndMT.

Homozygous *eNOS* mutant mice have been shown to exhibit several cardiovascular defects, including bicuspid aortic valves (Aicher et al., 2007; Feng et al., 2002; Lee et al., 2000). Interestingly, heterozygous *NOTCH1* mutations seen in humans are also associated with bicuspid aortic valves (Garg et al., 2005). Previous studies have shown that various signaling pathways can activate eNOS, in particular, shear stress is a major activator of NO generation (Cheng et al., 2005; Ziegler et al., 1998). Although it remains controversial whether heart development commences prior to blood flow (DeHaan, 1965) or whether blood flow is required to initiate the process (Hove et al., 2003; Nonaka et al., 2002), it is clear that narrowing at the AVC leads to increased shear stress at the endocardium at that location (Hove et al., 2003). Shear stress activates eNOS through phosphorylation of residue Ser1177 by Akt (Dimmeler et al., 1999; Fulton et al., 1999; Michell et al., 1999). Recent studies have suggested that shear stress also activates Notch signaling by inducing Notch receptors and ligands (Masumura et al., 2009; Wang et al., 2007). Thus, it is tempting to speculate that shear stress-induced NO may be in part through a Notch-dependent mechanism.

How then does Notch activate eNOS? Our data suggest that *INHBA* is a direct target gene of Notch, and that the INHBA homodimer, Activin A, is increased in NICD-conditioned medium (Figure 4B). Our studies confirm that *Inhba* is highly expressed in the AVC at E9.5 and E10.5 compared to the whole heart, and that Activin A appears to be the major paracrine factor in NICD-conditioned medium that activates the PI3K/Akt pathway and *eNOS*. Although members of the TGFβ superfamily are known critical factors in EndMT in the AVC (Nakajima et al., 2000), our results show a requirement for Activin A in particular.

Based on our results, we propose a model (see Graphical Abstract) where Notch-activated cells that become EndMT committed begin to lose cell-cell junctions (Niessen et al., 2008) and increase sGC levels. As these cells start to invade and migrate into the cardiac cushion, Notch-induced secretion of Activin A may diffuse into the surrounding endocardium to activate eNOS and induce NO synthesis. NO binding to sGC in the ECs committed to mesenchymal transition then promotes cell migration and invasion.

EXPERIMENTAL PROCEDURES

Animals

Male and female C57Bl/6J and eNOS null mice weighing between 25 and 35 g were purchased from Jackson Laboratories (Bar Harbor, ME). Tet^{OS}-dnMAML transgenic mice have been previously described (Fu et al., 2009). The VE-cadherin-tTA (VEtTA) strain was a gift from L. Benjamin, Harvard Medical School (Boston, MA) (Meadows et al., 2009). Suppression of dnMAML expression was achieved by administering either tetracycline (50 μg/ml) or doxycycline (50 μg/ml) in the drinking water. All animal protocols were approved by the Animal Care Committee of the University of British Columbia (Vancouver, British Columbia, Canada).

Reagents

Rabbit anti-GUCY1B3 was acquired from Abcam (Cambridge, MA). Rabbit anti-p-eNOS-S1177, rabbit anti-eNOS, rabbit anti-pAkt, rabbit anti-Akt, rabbit anti-cleaved Notch1 antibody, and LY294002 inhibitor were acquired from Cell Signaling Technology (Beverly, MA). Rat anti-RBPJ (RBPJk-T6719) was acquired from the Institute of Immunology, Tokyo (Hamaguchi et al., 1992). Rat anti-mouse CD31/PECAM antibody and type I collagen were acquired from BD Sciences (Franklin Lakes, NJ). Rabbit anti-GFP and Alexa Fluor secondary antibodies were acquired from Invitrogen (Carlsbad, CA). DAPI, mouse monoclonal antibody against the FLAG epitope (M2), mouse monoclonal antibody against Acta2, ODQ, L-NAME, Insulin/Transferrin/Selenium (ITS) supplement, and mouse anti-tubulin were purchased from Sigma-Aldrich (St. Louis, MO). DAR4M-AM was acquired from Millipore (Billerica, MA). The Griess reagent was obtained from Promega (Madison, WI). Neutralizing anti-Activin A antibody, Cyclic-GMP assay kit, and human Activin A (INHBA) Quantikine ELISA kit were purchased from R&D Systems (Minneapolis, MN). Human IGF2 ELISA kit was obtained from Diagnostic Systems Laboratories (Webster, TX). All primers were acquired from Integrated DNA Technologies (San Diego, CA). BAY41-2272 compound was purchased from Alexis/Enzo Life Sciences (Farmingdale, NY). DAPT and Akt inhibitor Triciribine were acquired from Calbiochem/EMD Chemicals (Gibbstown, NJ).

Cell Culture and RNA Interference

EC lines were obtained and cultured as previously described (Noseda et al., 2004). ECs were transduced using the retroviral vectors MIY, MIY-Jag1, MIY-Dll4, MIY-NICD, pLNCX, pLNCX-FLAG-RBPJ, MSCVNeo, and MSCVNeo-NICD as previously described (Niessen et al., 2008). pLNCX-AktDN-Myc (AktDN has been mutated to remove three activating phosphorylation sites, K179M, T308A, and S473A, and acts as a dn molecule) was a kind gift from Dr. Issei Komuro. Short hairpin RNA targeting *RBPJ*, *Gucy1b3*, *Inhba*, or random sequences were acquired from Open Biosystems (Huntsville, AL), or previously generated in-house (see Table S2) (Niessen et al., 2008). ECs were transduced with MSCVNeo-NICD or MSCVNeo to generate conditioned medium. All cells were starved in serum-free MCDB 131 medium for 24 hr prior to collection of conditioned medium. Conditioned medium was filtered with

(G–I) In vivo NO levels were measured by DAR4M-AM fluorescence (25 μmol/kg injected intraperitoneally 1 hr prior to collecting embryos) in E10.25 and E10.5 AVC from littermate control and VEtTAxTet^{OS}-dnMAML-GFP embryos following 24 hr of Notch inhibition (dnMAML induction). Representative sagittal sections are shown where the AVC border is outlined with white dotted lines. Mean DAR4M-AM staining intensities normalized to total AVC area (H) or total EC area (I) are shown (n = 4–7 with minimum 3 embryos per group; *$p \leq 0.05$).

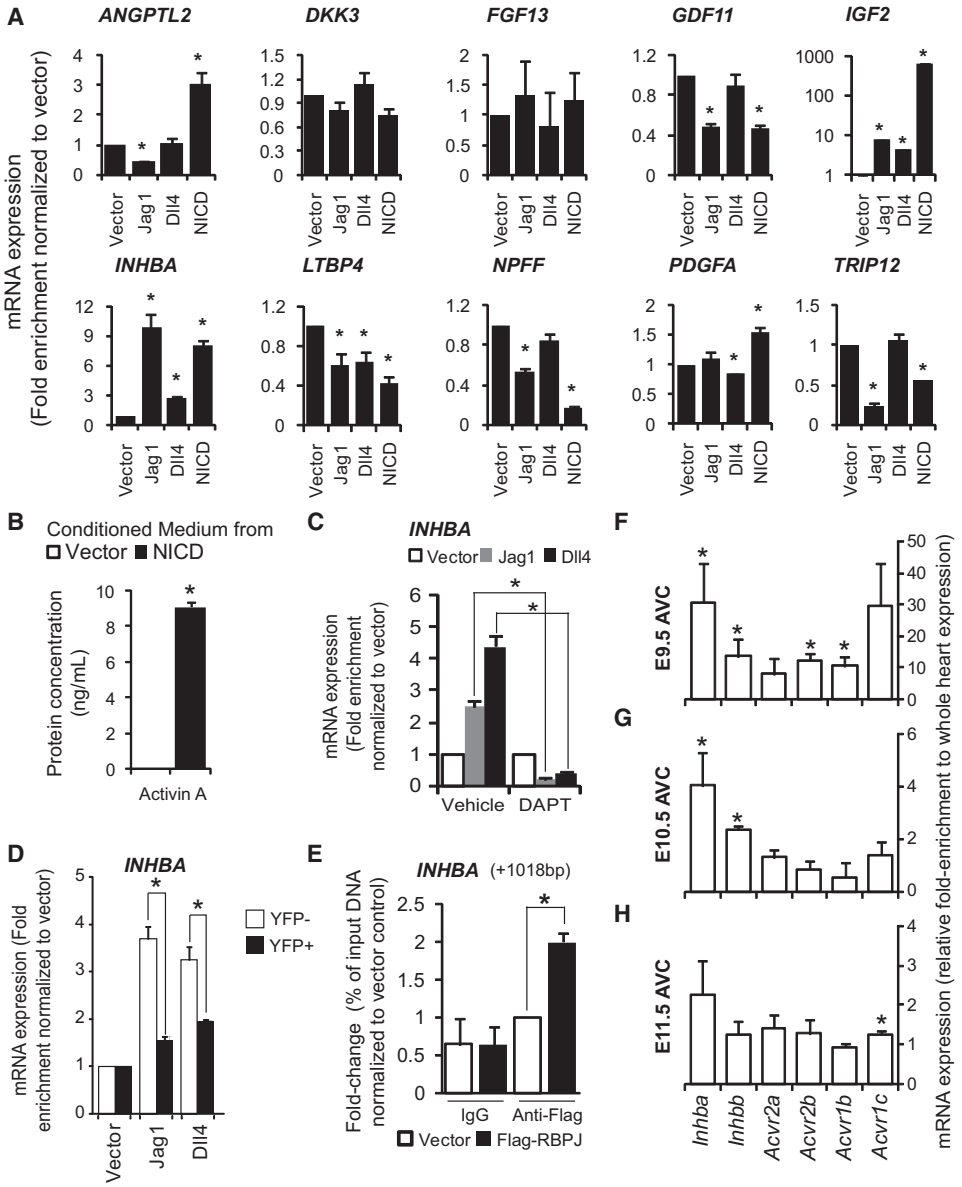

Figure 4. Notch Activation Induces *INHBA* Expression and Activin A Release

(A) Potential eNOS-activating factors were evaluated by RT-qPCR in Notch-activated ECs. ECs were transduced with Jag1, Dll4, NICD, or empty vector. Results are shown as fold enrichment over the vector control (n = 3; *p < 0.05).

(B) Activin A concentrations in empty vector- or NICD-transduced EC-conditioned medium were evaluated by ELISA and are shown (n = 9; *p = 0.001).

(C) Expression of *INHBA* in Notch ligand-activated ECs in the presence or absence of DAPT was evaluated by RT-qPCR, and data are shown as fold enrichment over the vector control (n = 3; *p < 0.0005).

(D) Expression of *INHBA* induced by Notch ligand was evaluated in flow-sorted Jag1, Dll4, or vector (YFP+), and cocultured parental ECs (YFP−) are shown as fold enrichment over the vector control (n = 3, *p < 0.05).

(E) RBPJ occupancy on a conserved putative RBPJ-binding site of human *INHBA* was examined by anti-Flag ChIP with IgG as negative control in ECs transduced with either Flag-RBPJ or empty vector. Fold enrichment is shown, determined as a percentage of input DNA and normalized to the empty vector anti-Flag ChIP (n = 3; *p = 0.05).

(F–H) RT-qPCR was used to analyze expression of *Inhba*, *Inhbb*, and their cognate receptors (*Acvr1* and *Acvr2*) at E9.5, E10.5, and E11.5 in the AVC and whole heart. Expression of genes in AVC is shown as fold enrichment over the whole heart at the same developmental stage (n = 3; *p = 0.05). Figure S4 shows Inhba expression by in situ hybridization.

a 0.45 μm filter and applied onto parental ECs, which were also starved in serum-free MCDB 131. All inhibitors and recombinant Activin A were added 1 hr prior to conditioned medium treatment. Cell lysates were collected in RIPA buffer as previously described (Fu et al., 2009).

Microarray and Analysis Software

HUVECs were either transduced with MIY-NICD or MIY vector control. The cells were sorted for YFP, and RNA was extracted using TRIzol (Invitrogen) and analyzed by the Affymetrix Human Genome U133 Plus 2.0 Array (NCBI

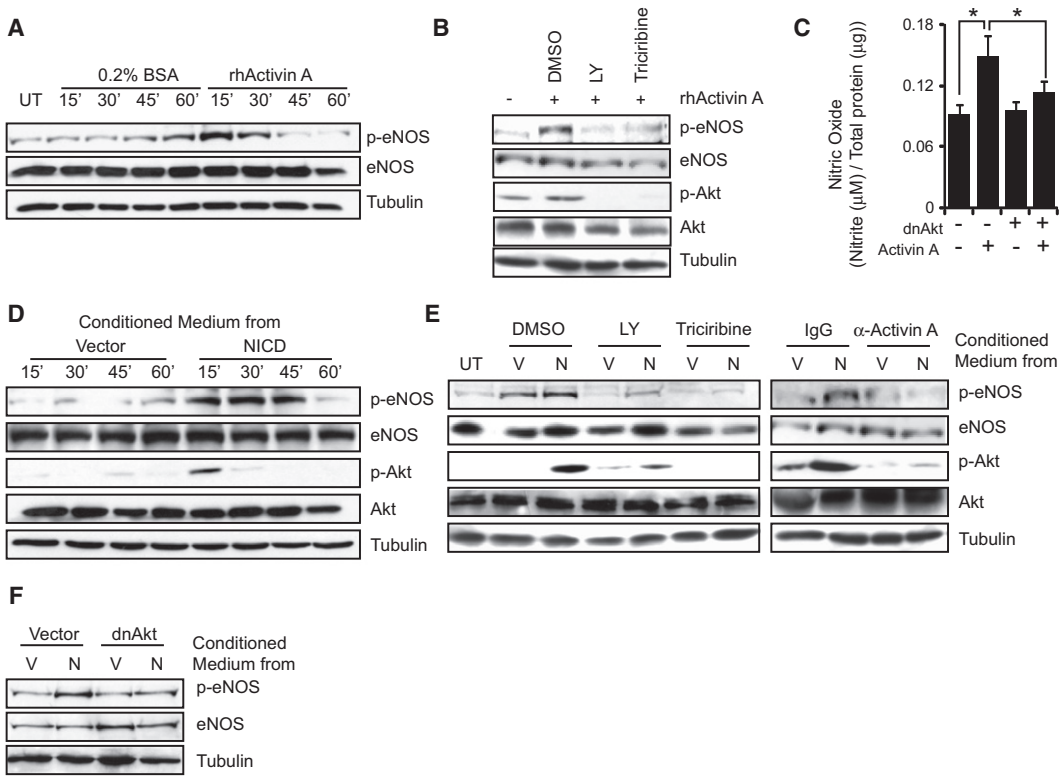

Figure 5. Notch-Induced Activin A Activates eNOS via the PI3K/Akt Pathway

(A) ECs were treated with either recombinant Activin A (5 ng/ml) or vehicle (0.2% BSA in PBS) for various times, and cell lysates were analyzed by immunoblotting for p-ENOS, ENOS, and Tubulin.

(B) Parental ECs were treated with recombinant Activin A (5 ng/ml) in the presence of vehicle (DMSO), PI3K inhibitor (LY294002, 10 μM), or Akt inhibitor (Triciribine, 10 μM) for 15 min, and cell lysates were analyzed by immunoblotting for p-ENOS, ENOS, p-Akt, Akt, and Tubulin.

(C) Mean nitrite levels as measured by the Griess reaction normalized to the total amount of protein in dnAkt or vector-transduced ECs treated with Activin A (n = 5; *p = 0.05).

(D) Parental ECs were treated with conditioned medium collected from either NICD-transduced or empty vector-transduced ECs for various times and cell lysates analyzed by immunoblotting using antibodies against the protein shown.

(E) Parental ECs were left untreated (UT), or treated with conditioned medium from either empty vector (V) or NICD (N)-transduced ECs in the presence of vehicle (DMSO), PI3K inhibitor (LY294002, 10 μM), or Akt inhibitor (Triciribine, 10 μM) for 15 min and examined by immunoblotting (left). Alternatively, conditioned medium from either empty vector (V)- or NICD (N)-transduced ECs was used to treat parental ECs in the presence of neutralizing anti-Activin A antibody or an IgG isotype control antibody (right).

(F) ECs transduced with either dnAkt or vector alone were treated with conditioned medium from either empty vector (V)- or NICD (N)-transduced ECs.

GEO accession number: GSE29850). Results were analyzed using the GCRMA algorithm to identify genes with a minimum of 2-fold induction as described (Harrington et al., 2008). SAGE libraries of the developing AVC were generated as part of the Mouse Atlas Project (Siddiqui et al., 2005) (www.mouseatlas.org). Gene ontology analysis was conducted using the DAVID/EASE program (Dennis et al., 2003).

RNA Collection and RT-qPCR

Total RNA from cultured cells or manually dissected C57BL/6J embryonic hearts was isolated by TRIzol isolation (Invitrogen), and cDNA was made as previously described (Noseda et al., 2004). RT-qPCR was carried out using the SYBR green (Applied Biosystems, Foster City, CA) method on an Applied Biosystems 7900HT with primers listed in Table S2. All primers targeting transcripts spanned exon-exon junctions were designed using the Roche ProbeLibrary website (Indianapolis, IN).

ChIP

ECs were transduced with pLNCX or pLNCX-FLAG-RBPJ, and the ChIP assay was performed as previously described (Noseda et al., 2004). ChIP DNA was amplified for *RBPJ*-binding sites in human *GUCY1A3*, *GUCY1B3*, *INHBA*, and *Hey1* promoters using primers listed in Table S2. Binding enrichment to the relevant promoter was calculated using the percentage of ChIP DNA (relative to input chromatin) normalized to the vector control.

Immunofluorescence Staining

Tissues were fixed in 4% paraformaldehyde (PFA) overnight, dehydrated in 30% sucrose/phosphate-buffered solution (PBS), and embedded in OCT (Sakura, Japan). Ten micron cryosections were collected and stored at −80°C until staining. For immunofluorescence staining, sections were washed with PBS and incubated overnight with primary antibody in staining buffer (4% calf serum/0.1%Triton X-100/PBS). Slides were then washed with PBS and incubated at room temperature with secondary antibodies in staining buffer for 1 hr. Slides were then washed with PBS, and nuclei were stained with DAPI and mounted with ProLong Gold Antifade (Invitrogen). All AVC micrographs were acquired using an Axiovert S100 Zeiss microscope. Images were captured using NorthernEclipse software and quantifications performed using ImageJ (NIH).

AVC Explant Assay

AVC explant assays were performed as previously described (Niessen et al., 2008). Explants were cultured for 48 hr with various inhibitors or activators in 1% FBS/0.5% ITS/DMEM: γ-secretase inhibitor (DAPT, 10 μM), sGC inhibitor

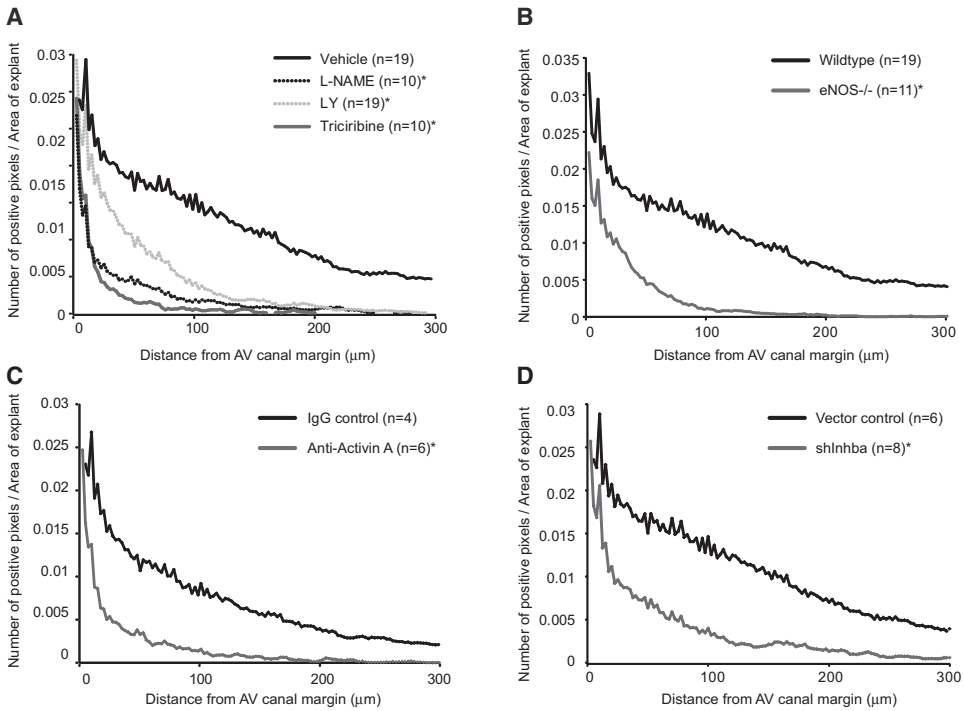

Figure 6. The Notch-Activin A-PI3K/Akt-eNOS Axis Is Necessary for AVC EndMT

Quantitative analysis of EndMT in AVC explants from E9.5 AVC.

(A) Nitric oxide signaling-induced EndMT was evaluated by treating AVC with inhibitors L-NAME (50 μM), LY294002 (10 μM), Triciribine (10 μM), or DMSO (vehicle).

(B) AVCs from eNOS$^{-/-}$ mice or wild-type controls were quantified for EndMT.

(C) The requirement for Activin A in EndMT was evaluated by treating AVC with either anti-Activin A neutralizing antibody (0.5 ng/ml) or isotype control IgG.

(D) Alternatively, wild-type AVCs were lentivirally transduced with shInhba to knock down *Inhba*, or a vector control. Results represent the distance migrated of cells invading the collagen matrix from the edge of the AVC explant normalized to the area of the AVC tissue (*p = 0.05). See also Figure S5 for correlation with Acta2 staining.

(ODQ, 10 μM), NO-independent sGC activator (BAY41-2272, 10 μM), NOS inhibitor (L-NAME, 50 μM), PI3K inhibitor LY294002 (10 μM), Akt inhibitor Triciribine (10 μM), anti-Activin A neutralizing antibody (0.5 mg/ml), isotype IgG control (0.5 mg/ml) or purified lentivirus targeting *Gucy1b3*, *Inhba* or vector control. Explants were fixed with 4% PFA and then stained for *Acta2* and DAPI. All immunofluorescence micrographs were acquired using an Axioplan2 Zeiss microscope. The number and distance of migrating cells were analyzed as previously described (Niessen et al., 2008). Briefly, *Acta2* or DAPI staining pixels were summed up for each pixel that was closest to the AVC explant. This was repeated by extending one pixel away from the explant until all migrating and invading cells were accounted for. All readings were then normalized to size of AVC explant and plotted over distance (Supplemental Experimental Procedures). To ensure that the migrating/invading cells comprised mesenchymal cells, all explants were also stained with the mesenchymal marker, Acta2, and the areas of Acta2 and DAPI staining were correlated (Supplemental Experimental Procedures, and Figures S3 and S5).

Data Analysis

All data are shown as the mean ± SEM of multiple experiments. All statistical analyses were calculated using two-tailed Student's t test and were considered to be statistically significant at $p < 0.05$.

SUPPLEMENTAL INFORMATION

Supplemental Information includes five figures, two tables, and Supplemental Experimental Procedures and can be found with this article online at doi:10.1016/j.devcel.2011.06.022.

ACKNOWLEDGMENTS

This research was supported by grants to A. Karsan from the Canadian Institutes of Health Research (MOP 64354) and the Heart and Stroke Foundation of British Columbia and the Yukon and grants to A. Karsan, P.A.H., and M.M. from Genome Canada and Genome British Columbia. A. Karsan, P.A.H., and M.M. are Senior Scholars of the Michael Smith Foundation for Health Research. We thank Denise McDougal and Fred Wong for assistance with flow cytometry and cell sorting.

Received: September 10, 2010
Revised: April 20, 2011
Accepted: June 17, 2011
Published online: August 15, 2011

REFERENCES

Aicher, D., Urbich, C., Zeiher, A., Dimmeler, S., and Schäfers, H.J. (2007). Endothelial nitric oxide synthase in bicuspid aortic valve disease. Ann. Thorac. Surg. *83*, 1290–1294.

Arrington, C.B., and Yost, H.J. (2009). Extra-embryonic syndecan 2 regulates organ primordia migration and fibrillogenesis throughout the zebrafish embryo. Development *136*, 3143–3152.

Baker, D.A., and Kelly, J.M. (2004). Structure, function and evolution of microbial adenylyl and guanylyl cyclases. Mol. Microbiol. *52*, 1229–1242.

Camenisch, T.D., Molin, D.G., Person, A., Runyan, R.B., Gittenberger-de Groot, A.C., McDonald, J.A., and Klewer, S.E. (2002). Temporal and distinct

TGFbeta ligand requirements during mouse and avian endocardial cushion morphogenesis. Dev. Biol. *248*, 170–181.

Cheng, C., van Haperen, R., de Waard, M., van Damme, L.C., Tempel, D., Hanemaaijer, L., van Cappellen, G.W., Bos, J., Slager, C.J., Duncker, D.J., et al. (2005). Shear stress affects the intracellular distribution of eNOS: direct demonstration by a novel in vivo technique. Blood *106*, 3691–3698.

DeHaan, R.L. (1965). Development of pacemaker tissue in the embryonic heart. Ann. N Y Acad. Sci. *127*, 7–18.

Dennis, G., Jr., Sherman, B.T., Hosack, D.A., Yang, J., Gao, W., Lane, H.C., and Lempicki, R.A. (2003). DAVID: Database for Annotation, Visualization, and Integrated Discovery. Genome Biol. *4*, 3.

Dimmeler, S., Fleming, I., Fisslthaler, B., Hermann, C., Busse, R., and Zeiher, A.M. (1999). Activation of nitric oxide synthase in endothelial cells by Akt-dependent phosphorylation. Nature *399*, 601–605.

Donovan, J., Kordylewska, A., Jan, Y.N., and Utset, M.F. (2002). Tetralogy of fallot and other congenital heart defects in Hey2 mutant mice. Curr. Biol. *12*, 1605–1610.

Eisenberg, L.M., and Markwald, R.R. (1995). Molecular regulation of atrioventricular valvuloseptal morphogenesis. Circ. Res. *77*, 1–6.

Eldadah, Z.A., Hamosh, A., Biery, N.J., Montgomery, R.A., Duke, M., Elkins, R., and Dietz, H.C. (2001). Familial Tetralogy of Fallot caused by mutation in the jagged1 gene. Hum. Mol. Genet. *10*, 163–169.

Feng, Q., Song, W., Lu, X., Hamilton, J.A., Lei, M., Peng, T., and Yee, S.P. (2002). Development of heart failure and congenital septal defects in mice lacking endothelial nitric oxide synthase. Circulation *106*, 873–879.

Feng, Q., Di, R., Tao, F., Chang, Z., Lu, S., Fan, W., Shan, C., Li, X., and Yang, Z. (2010). PDK1 regulates vascular remodeling and promotes epithelial-mesenchymal transition in cardiac development. Mol. Cell. Biol. *30*, 3711–3721.

Fischer, A., Schumacher, N., Maier, M., Sendtner, M., and Gessler, M. (2004). The Notch target genes Hey1 and Hey2 are required for embryonic vascular development. Genes Dev. *18*, 901–911.

Fischer, A., Steidl, C., Wagner, T.U., Lang, E., Jakob, P.M., Friedl, P., Knobeloch, K.P., and Gessler, M. (2007). Combined loss of Hey1 and HeyL causes congenital heart defects because of impaired epithelial to mesenchymal transition. Circ. Res. *100*, 856–863.

Friebe, A., Mergia, E., Dangel, O., Lange, A., and Koesling, D. (2007). Fatal gastrointestinal obstruction and hypertension in mice lacking nitric oxide-sensitive guanylyl cyclase. Proc. Natl. Acad. Sci. USA *104*, 7699–7704.

Fu, Y., Chang, A., Chang, L., Niessen, K., Eapen, S., Setiadi, A., and Karsan, A. (2009). Differential regulation of transforming growth factor beta signaling pathways by Notch in human endothelial cells. J. Biol. Chem. *284*, 19452–19462.

Fukumura, D., Kashiwagi, S., and Jain, R.K. (2006). The role of nitric oxide in tumour progression. Nat. Rev. Cancer *6*, 521–534.

Fulton, D., Gratton, J.P., McCabe, T.J., Fontana, J., Fujio, Y., Walsh, K., Franke, T.F., Papapetropoulos, A., and Sessa, W.C. (1999). Regulation of endothelium-derived nitric oxide production by the protein kinase Akt. Nature *399*, 597–601.

Garg, V., Muth, A.N., Ransom, J.F., Schluterman, M.K., Barnes, R., King, I.N., Grossfeld, P.D., and Srivastava, D. (2005). Mutations in NOTCH1 cause aortic valve disease. Nature *437*, 270–274.

Giuili, G., Scholl, U., Bulle, F., and Guellaën, G. (1992). Molecular cloning of the cDNAs coding for the two subunits of soluble guanylyl cyclase from human brain. FEBS Lett. *304*, 83–88.

Groneberg, D., König, P., Wirth, A., Offermanns, S., Koesling, D., and Friebe, A. (2010). Smooth muscle-specific deletion of nitric oxide-sensitive guanylyl cyclase is sufficient to induce hypertension in mice. Circulation *121*, 401–409.

Hamaguchi, Y., Yamamoto, Y., Iwanari, H., Maruyama, S., Furukawa, T., Matsunami, N., and Honjo, T. (1992). Biochemical and immunological characterization of the DNA binding protein (RBP-J kappa) to mouse J kappa recombination signal sequence. J. Biochem. *112*, 314–320.

Harrington, L.S., Sainson, R.C., Williams, C.K., Taylor, J.M., Shi, W., Li, J.L., and Harris, A.L. (2008). Regulation of multiple angiogenic pathways by Dll4 and Notch in human umbilical vein endothelial cells. Microvasc. Res. *75*, 144–154.

High, F.A., and Epstein, J.A. (2008a). The multifaceted role of Notch in cardiac development and disease. Nat. Rev. Genet. *9*, 49–61.

High, F.A., Lu, M.M., Pear, W.S., Loomes, K.M., Kaestner, K.H., and Epstein, J.A. (2008b). Endothelial expression of the Notch ligand Jagged1 is required for vascular smooth muscle development. Proc. Natl. Acad. Sci. USA *105*, 1955–1959.

Hove, J.R., Köster, R.W., Forouhar, A.S., Acevedo-Bolton, G., Fraser, S.E., and Gharib, M. (2003). Intracardiac fluid forces are an essential epigenetic factor for embryonic cardiogenesis. Nature *421*, 172–177.

Ignarro, L.J., Harbison, R.G., Wood, K.S., and Kadowitz, P.J. (1986). Activation of purified soluble guanylate cyclase by endothelium-derived relaxing factor from intrapulmonary artery and vein: stimulation by acetylcholine, bradykinin and arachidonic acid. J. Pharmacol. Exp. Ther. *237*, 893–900.

Iso, T., Kedes, L., and Hamamori, Y. (2003). HES and HERP families: multiple effectors of the Notch signaling pathway. J. Cell. Physiol. *194*, 237–255.

Lee, T.C., Zhao, Y.D., Courtman, D.W., and Stewart, D.J. (2000). Abnormal aortic valve development in mice lacking endothelial nitric oxide synthase. Circulation *101*, 2345–2348.

Li, L., Krantz, I.D., Deng, Y., Genin, A., Banta, A.B., Collins, C.C., Qi, M., Trask, B.J., Kuo, W.L., Cochran, J., et al. (1997). Alagille syndrome is caused by mutations in human Jagged1, which encodes a ligand for Notch1. Nat. Genet. *16*, 243–251.

Luna-Zurita, L., Prados, B., Grego-Bessa, J., Luxán, G., del Monte, G., Benguría, A., Adams, R.H., Pérez-Pomares, J.M., and de la Pompa, J.L. (2010). Integration of a Notch-dependent mesenchymal gene program and Bmp2-driven cell invasiveness regulates murine cardiac valve formation. J. Clin. Invest. *120*, 3493–3507.

Masumura, T., Yamamoto, K., Shimizu, N., Obi, S., and Ando, J. (2009). Shear stress increases expression of the arterial endothelial marker ephrinB2 in murine ES cells via the VEGF-Notch signaling pathways. Arterioscler. Thromb. Vasc. Biol. *29*, 2125–2131.

Meadows, K.N., Iyer, S., Stevens, M.V., Wang, D., Shechter, S., Perruzzi, C., Camenisch, T.D., and Benjamin, L.E. (2009). Akt promotes endocardial-mesenchyme transition. J. Angiogenes. Res. *1*, 2.

Mergia, E., Russwurm, M., Zoidl, G., and Koesling, D. (2003). Major occurrence of the new alpha2beta1 isoform of NO-sensitive guanylyl cyclase in brain. Cell. Signal. *15*, 189–195.

Mergia, E., Friebe, A., Dangel, O., Russwurm, M., and Koesling, D. (2006). Spare guanylyl cyclase NO receptors ensure high NO sensitivity in the vascular system. J. Clin. Invest. *116*, 1731–1737.

Michell, B.J., Griffiths, J.E., Mitchelhill, K.I., Rodriguez-Crespo, I., Tiganis, T., Bozinovski, S., de Montellano, P.R., Kemp, B.E., and Pearson, R.B. (1999). The Akt kinase signals directly to endothelial nitric oxide synthase. Curr. Biol. *9*, 845–848.

Mount, P.F., Kemp, B.E., and Power, D.A. (2007). Regulation of endothelial and myocardial NO synthesis by multi-site eNOS phosphorylation. J. Mol. Cell. Cardiol. *42*, 271–279.

Murad, F. (1986). Cyclic guanosine monophosphate as a mediator of vasodilation. J. Clin. Invest. *78*, 1–5.

Nakajima, Y., Yamagishi, T., Hokari, S., and Nakamura, H. (2000). Mechanisms involved in valvuloseptal endocardial cushion formation in early cardiogenesis: roles of transforming growth factor (TGF)-beta and bone morphogenetic protein (BMP). Anat. Rec. *258*, 119–127.

Niessen, K., and Karsan, A. (2008). Notch signaling in cardiac development. Circ. Res. *102*, 1169–1181.

Niessen, K., Fu, Y., Chang, L., Hoodless, P.A., McFadden, D., and Karsan, A. (2008). Slug is a direct Notch target required for initiation of cardiac cushion cellularization. J. Cell Biol. *182*, 315–325.

Nonaka, S., Shiratori, H., Saijoh, Y., and Hamada, H. (2002). Determination of left-right patterning of the mouse embryo by artificial nodal flow. Nature *418*, 96–99.

Noseda, M., McLean, G., Niessen, K., Chang, L., Pollet, I., Montpetit, R., Shahidi, R., Dorovini-Zis, K., Li, L., Beckstead, B., et al. (2004). Notch activation results in phenotypic and functional changes consistent with endothelial-to-mesenchymal transformation. Circ. Res. *94*, 910–917.

Oda, T., Elkahloun, A.G., Pike, B.L., Okajima, K., Krantz, I.D., Genin, A., Piccoli, D.A., Meltzer, P.S., Spinner, N.B., Collins, F.S., and Chandrasekharappa, S.C. (1997). Mutations in the human Jagged1 gene are responsible for Alagille syndrome. Nat. Genet. *16*, 235–242.

Pyriochou, A., Beis, D., Koika, V., Potytarchou, C., Papadimitriou, E., Zhou, Z., and Papapetropoulos, A. (2006). Soluble guanylyl cyclase activation promotes angiogenesis. J. Pharmacol. Exp. Ther. *319*, 663–671.

Pyriochou, A., Vassilakopoulos, T., Zhou, Z., and Papapetropoulos, A. (2007a). cGMP-dependent and -independent angiogenesis-related properties of nitric oxide. Life Sci. *81*, 1549–1554.

Pyriochou, A., Zhou, Z., Koika, V., Petrou, C., Cordopatis, P., Sessa, W.C., and Papapetropoulos, A. (2007b). The phosphodiesterase 5 inhibitor sildenafil stimulates angiogenesis through a protein kinase G/MAPK pathway. J. Cell. Physiol. *211*, 197–204.

Rastaldo, R., Pagliaro, P., Cappello, S., Penna, C., Mancardi, D., Westerhof, N., and Losano, G. (2007). Nitric oxide and cardiac function. Life Sci. *81*, 779–793.

Sessa, W.C. (2009). Molecular control of blood flow and angiogenesis: role of nitric oxide. J. Thromb. Haemost. *7* (*Suppl 1*), 35–37.

Siddiqui, A.S., Khattra, J., Delaney, A.D., Zhao, Y., Astell, C., Asano, J., Babakaiff, R., Barber, S., Beland, J., Bohacec, S., et al. (2005). A mouse atlas of gene expression: large-scale digital gene-expression profiles from precisely defined developing C57BL/6J mouse tissues and cells. Proc. Natl. Acad. Sci. USA *102*, 18485–18490.

Sun, D., Mcalmon, K.R., Davies, J.A., Bernfield, M., and Hay, E.D. (1998). Simultaneous loss of expression of syndecan-1 and E-cadherin in the embryonic palate during epithelial-mesenchymal transformation. Int. J. Dev. Biol. *42*, 733–736.

Timmerman, L.A., Grego-Bessa, J., Raya, A., Bertrán, E., Pérez-Pomares, J.M., Díez, J., Aranda, S., Palomo, S., McCormick, F., Izpisúa-Belmonte, J.C., and de la Pompa, J.L. (2004). Notch promotes epithelial-mesenchymal transition during cardiac development and oncogenic transformation. Genes Dev. *18*, 99–115.

Vrljicak, P., Chang, A.C., Morozova, O., Wederell, E.D., Niessen, K., Marra, M.A., Karsan, A., and Hoodless, P.A. (2010). Genomic analysis distinguishes phases of early development of the mouse atrio-ventricular canal. Physiol. Genomics *40*, 150–157.

Vyas-Read, S., Shaul, P.W., Yuhanna, I.S., and Willis, B.C. (2007). Nitric oxide attenuates epithelial-mesenchymal transition in alveolar epithelial cells. Am. J. Physiol. Lung Cell. Mol. Physiol. *293*, L212–L221.

Wang, X.L., Fu, A., Raghavakaimal, S., and Lee, H.C. (2007). Proteomic analysis of vascular endothelial cells in response to laminar shear stress. Proteomics *7*, 588–596.

Yamagami, S., and Suzuki, N. (2005). Diverse forms of guanylyl cyclases in medaka fish — their genomic structure and phylogenetic relationships to those in vertebrates and invertebrates. Zoolog. Sci. *22*, 819–835.

Ziegler, T., Silacci, P., Harrison, V.J., and Hayoz, D. (1998). Nitric oxide synthase expression in endothelial cells exposed to mechanical forces. Hypertension *32*, 351–355.